

## Article

# Effect of Target Sintering Temperature on the Morphological and Optical Properties of Pulsed Laser Deposited TiO<sub>2</sub> Thin Films

Laid Kadri <sup>1,\*</sup> , Georgiana Bulai <sup>2</sup> , Aurelian Carlescu <sup>2,\*</sup>, Stoian George <sup>3</sup> , Silviu Gurlui <sup>4</sup>, Liviu Leontie <sup>2,5</sup>, Corneliu Doroftei <sup>2</sup> and Mohamed Adnane <sup>1</sup>

- <sup>1</sup> Laboratoire de Microscopie Electronique et Sciences des Matériaux (LMESM), Département de Technologie des Matériaux, Faculté de Physique, Université des Sciences et de la Technologie d'Oran Mohamed Boudiaf (USTO-MB), El M'naouar BP 1505, Bir El Djir, Oran 31000, Algeria; mohamed67adnane@gmail.com
- <sup>2</sup> Science Research Department, Institute of Interdisciplinary Research, Research Center in Environmental Sciences for the North-Eastern Romanian Region (CERNESIM), Alexandru Ioan Cuza University of Iasi, Bulevardul Carol I, Nr. 11, 700506 Iasi, Romania; georgiana.bulai@uaic.ro (G.B.); lleontie@uaic.ro (L.L.); corneliu.doroftei@uaic.ro (C.D.)
- <sup>3</sup> National Institute of Research and Development for Technical Physics, 47 Mangeron Boulevard, 700050 Iasi, Romania; gstoian@phys-iasi.ro
- <sup>4</sup> LOA-SL, Faculty of Physics, Alexandru Ioan Cuza University of Iasi, Bulevardul Carol I, Nr. 11, 700506 Iasi, Romania; sgurlui@uaic.ro
- <sup>5</sup> Faculty of Physics, Alexandru Ioan Cuza University of Iasi, Bulevardul Carol I, Nr. 11, 700506 Iasi, Romania
- \* Correspondence: laid.kadri@univ-usto.dz (L.K.); aurelian.carlescu@uaic.ro (A.C.)



**Citation:** Kadri, L.; Bulai, G.; Carlescu, A.; George, S.; Gurlui, S.; Leontie, L.; Doroftei, C.; Adnane, M. Effect of Target Sintering Temperature on the Morphological and Optical Properties of Pulsed Laser Deposited TiO<sub>2</sub> Thin Films. *Coatings* **2021**, *11*, 561. <https://doi.org/10.3390/coatings11050561>

Academic Editor: Chen Tei-Chen

Received: 31 March 2021

Accepted: 6 May 2021

Published: 11 May 2021

**Publisher's Note:** MDPI stays neutral with regard to jurisdictional claims in published maps and institutional affiliations.



**Copyright:** © 2021 by the authors. Licensee MDPI, Basel, Switzerland. This article is an open access article distributed under the terms and conditions of the Creative Commons Attribution (CC BY) license (<https://creativecommons.org/licenses/by/4.0/>).

**Abstract:** In this paper, we report on the effect of titanium dioxide (TiO<sub>2</sub>) target sintering temperature on the morphological and optical properties of amorphous titanium dioxide thin films synthesized by pulsed laser deposition (PLD) on indium tin oxide (ITO) glass substrate and subsequently heat-treated in air at low temperature (150 °C). Three types of targets were used, unsintered (pressed at room temperature), sintered at 500 °C and sintered at 1000 °C. The surface morphology of the samples was investigated by scanning electron microscopy (SEM), and profilometry was used for thickness measurements. The structural properties of the films were examined by X-ray diffraction (XRD), while their optical properties were studied by UV-vis spectroscopy. The obtained TiO<sub>2</sub> thin films have an amorphous nature, as shown by XRD analysis. Profilometer showed that sintered target samples have more reliable thicknesses than unsintered ones. The SEM studies revealed the sufficient structural homogeneity of sintered target nanosized TiO<sub>2</sub> films and agglomerates in the case of unsintered target film. The UV-vis transmittance spectra showed high transparency in the visible range of PLD films, proportional to the target sintering temperature. The optical band gaps of the films deposited using the 500 °C and 1000 °C sintered targets are closer to those of anatase and rutile phases, respectively, which provides a promising approach to the challenges of amorphous TiO<sub>2</sub>-based nanostructures.

**Keywords:** TiO<sub>2</sub>; thin films; amorphous; PLD; target; sintering

## 1. Introduction

Titanium dioxide (TiO<sub>2</sub>) in thin films has been extensively used in a wide range of applications, such as sensors, self-cleaning, protective or antireflective layers, electrodes in electrochromic devices, electron transport layers in emerging photovoltaic cells (dye-sensitized, perovskite and polymeric cells), photocatalysts, pigments, etc., due to its high transparency across the visible spectrum, appropriate band gap, effective charge separation ability, low toxicity and low price [1–8]. Titanium dioxide (titania) also displays abundant surface hydroxyl (OH) groups, high defect density and enhanced absorption in the ultraviolet (UV) range, such as UV materials [9–13].

Titania is a *n*-type semiconductor material and displays three stable polymorphic forms: anatase (tetragonal), rutile (tetragonal) and brookite (orthorhombic) phases, which provide flexibility and versatility in applications [8,14]. At increased temperatures (~500 °C), amorphous TiO<sub>2</sub> transforms to crystalline anatase, and at temperatures higher than about ~700 °C to 800 °C, to rutile phase. The transformation to rutile phase is irreversible, and the melting point of TiO<sub>2</sub> is 1858 °C [8,14,15]. Furthermore, the currently known methods to crystallize amorphous TiO<sub>2</sub> films into anatase or rutile phases require the annealing step, including oxygen plasma treatment [16–18]. Anatase crystals exhibit excellent optical properties, higher photocatalytic activity and gas sensing properties than rutile ones, and a lower electron–hole recombination rate. Further, the band gap of anatase phase (3.2 eV) is larger than that of rutile (3.0 eV), and the charge carrier mobility is higher [16,19]. However, rutile phase is more thermodynamically stable and durable than anatase, while brookite is not commonly studied because it is difficult to prepare due to its metastability [15,20,21]. The transport mechanism of carriers (electrons and holes) in titania can be improved in the case of mixed-phase TiO<sub>2</sub> (rutile-anatase), which exhibits higher photocatalytic activity [16].

Although amorphous TiO<sub>2</sub> films have numerous advantages, including simple synthesis conditions and a larger surface area, allowing the integration of more chemicals and compatibility with the largest variety of substrates [1,22], they are much less studied compared to crystalline (anatase or rutile phases) films. In addition, the oxygen vacancies and disordered arrangement of intrinsic atoms have important effects on the electronic structure, which could improve the separation efficiency and transfer of photogenerated charge carriers [22–24]. Moreover, the electronic structure and optical properties of amorphous TiO<sub>2</sub> are much closer to those of anatase TiO<sub>2</sub> [24]. A new approach to TiO<sub>2</sub> thin film exploration and applications was provided by Addonizio et al. [1], Kim et al. [17] and Sun et al. [24].

Various methods have been used to obtain TiO<sub>2</sub> thin films, such as electron beam evaporation [25], radiofrequency (RF) magnetron sputtering [26], chemical vapor deposition [27], sol–gel technique [28], and pulsed laser deposition (PLD) [29,30]. The properties of deposited films are highly dependent on the processing techniques and the deposition conditions [31]. Pulsed laser deposition offers several benefits: the simple system operation, flexibility, a wide range of deposition conditions, rich choice of materials, the possibility to use in situ heating and reactive background gases, and a relatively high reproducibility [8,19,32,33]. This technique also allows the deposition of films with determined thickness, morphology, stoichiometry, grain size and composition by varying the deposition parameters (laser pulse geometry, laser fluence, wavelength or repetition frequency, target-substrate distance, substrate temperature, deposition time, etc.) [11,34,35]. The composition, purity and density (sintering temperature) of the bulk target have an important influence on the quality of laser ablated films [36]. Furthermore, in vacuum, PLD provides compact and continuous films, whereas porous structures can be achieved at relatively high background gas pressures [37].

In this study, we report the successful synthesis of nanosized amorphous TiO<sub>2</sub> films by PLD on indium tin oxide (ITO) glass substrate (due to their high visible transmittance, among transparent conducting oxides materials [38]) at room temperature (25 °C), without reactive background gases, from two targets sintered at different temperatures (500 °C and 1000 °C) and an unsintered one (25 °C), as-deposited films were then thermally treated at 150 °C for 30 min. The study of PLD-synthesized amorphous nanosized TiO<sub>2</sub> thin films is still poorly reported in the literature. The influence of target sintering temperature on the morphological and optical properties was investigated by scanning electron microscopy (SEM) and UV-vis spectroscopy, respectively. The obtained thin films may not only display a satisfactory uniformity and highly transparent TiO<sub>2</sub> nanostructures via low-temperature processing, but also exhibit similar optical properties to those of crystalline TiO<sub>2</sub>.

## 2. Experimental Details

The experimental setup used for pulsed laser deposition of TiO<sub>2</sub> films is similar to that described in [39]. The disk-shaped targets with ~20 mm diameter and about 2 mm thickness were prepared from commercially available high purity (>99.50%) titanium (IV) oxide powder (BIOCHEM Chemopharma; product code: 320150500). The powder was ground in an agate mortar and pressed at 2 MPa. Three targets were used for deposition: one target was prepared at room temperature (25 °C), while two others were sintered in air for 5 h (one at 500 °C and the second at 1000 °C, both with a 10 °C/min heating rate), using a Apriltherm 5L furnace. The films were deposited on ITO (thickness: ~150 nm, sheet resistance: ~10 Ω/sq, transmittance > 80% and with (400) texture)-coated glass substrates (10 mm × 15 mm × 1 mm), which were ultrasonically cleaned using acetone for 10 min and dried in air before loading them into the PLD chamber. Three thin-film samples were used, labeled as *as 25-TiO<sub>2</sub>*, *as 500-TiO<sub>2</sub>* and *as 1000-TiO<sub>2</sub>*, according to the target sintering temperature. All the depositions were performed at room temperature without reactive background gases, using the experimental parameters shown in Table 1. The targets were rotated during the laser irradiation in order to avoid the formation of deep surface craters [16]. Thermal treatments (5 °C/min heating rate, 30 min dwell at 150 °C) were performed ex situ on the as-deposited samples to ensure good adherence and compactness, and to moderate the transmittance of the titania films. Heat-treated samples were labeled similarly, as *ptt 25-TiO<sub>2</sub>*, *ptt 500-TiO<sub>2</sub>* and *ptt 1000-TiO<sub>2</sub>*.

**Table 1.** Deposition parameters used for the nanosized TiO<sub>2</sub> film preparation.

Lasers	Nd:YAG, 2nd Harmonic, λ = 532 nm
Pulse duration	10 ns
Repetition rate	10 Hz
Pulse energy	50 mJ/pulse
Spot size	~2.5 mm <sup>2</sup>
Fluence	2.0 J/cm <sup>2</sup>
Target	TiO <sub>2</sub> , sintered at 25 °C, 500 °C, and 1000 °C
Substrate	ITO glass
Target-substrate distance	50 mm
Pressure	50 mTorr
Deposition time	10 min

The thickness of thin-film samples under study was measured with a Dektak XT stylus profilometer (Bruker, Paris, France) with a resolution of 1 nm, while the morphological properties of the films were studied by SEM (JSM 6390/JEOL apparatus at 30 kV accelerating voltage). The UV-vis transmittance spectra of the films in the 300–900 nm wavelength range were recorded using a UV-vis Avantes spectrometer (AvaSpec 2048, Schiphol, The Netherlands). The XRD patterns in the 10–80° 2θ range were obtained using a Shimadzu LabX XRD-6000 diffractometer (Shimadzu, Kyoto, Japan) with a CuK<sub>α</sub> radiation (λ = 1.54 Å) and further used in structural analysis of samples. The diffractograms were recorded with a scanning angle step of 0.02° and 1°/min scan speed.

## 3. Results and Discussion

### 3.1. Morphological Properties

Figure 1 shows the influence of target sintering temperature on the film thickness. The thickness of three thin-film samples, *as 25-TiO<sub>2</sub>*, *as 500-TiO<sub>2</sub>* and *as 1000-TiO<sub>2</sub>*, were found to be approximately equal to 67, 47 and 34 nm, respectively. The lower thickness of the *as 500-TiO<sub>2</sub>* and *as 1000-TiO<sub>2</sub>* films compared to that of *as 25-TiO<sub>2</sub>* one could be due to the greater density (high sintered temperature) of sintered targets compared to that of the unsintered one (i.e., the films obtained from higher density targets are more compact than those prepared from the sparse one, containing agglomerations, which can affect the accuracy of the film thickness measurement). However, the films obtained from sintered

targets had slight differences in the thickness. Consequently, the thicknesses of sintered targets films were determined more accurately than in the case of unsintered one.

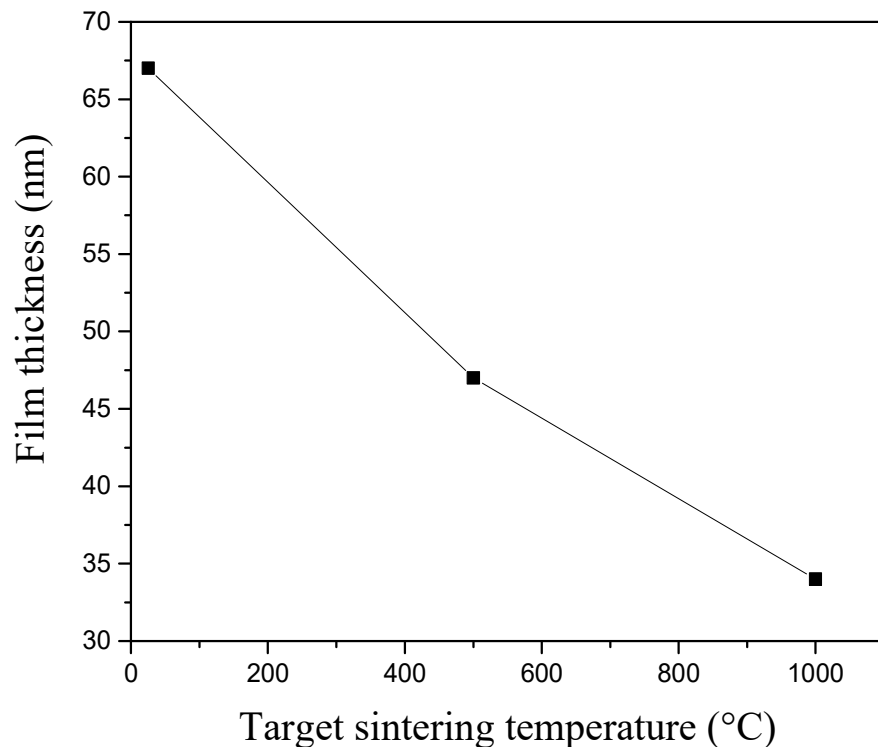


**Figure 1.** Target sintering temperature influence on thin-film thickness.

Scanning electron microscopy micrographs of  $\text{TiO}_2$  samples grown on ITO glass substrates were acquired to study the thin-film morphology (Figure 2). The *as 25-TiO<sub>2</sub>* (Figure 2a) film displays a granular structure, with significant agglomerates (white particulates) and weak small cracks. The *as 500-TiO<sub>2</sub>* (Figure 2b) and *as 1000-TiO<sub>2</sub>* (Figure 2c) samples display relatively uniform and flat surfaces composed of small irregular-shaped grains, with slight agglomerates in the case of *as 500-TiO<sub>2</sub>*. The presence of agglomerates can be attributed to the sparse target or lower density [36]. However, the reason for these small cracks is still not very clear. They may result from the presence of agglomerates combined with lower thickness of the film (i.e., in some cases, the particulates larger than film thickness, as shown by profilometry, can affect the film adhesion).

After thermal treatment for 30 min at 150 °C, the *ptt 25-TiO<sub>2</sub>* (Figure 2d), *ptt 500-TiO<sub>2</sub>* (Figure 2e) and *ptt 1000-TiO<sub>2</sub>* (Figure 2f) films were not distinctively changed, except for the reduction in agglomerates. The morphology of the agglomerates was influenced by the heat treatment, resulting in a reduction [40], while the slight change in the films morphology is due to the low temperature treatment [1,41].

### 3.2. Structural Properties

Figure 3a shows the XRD patterns of  $\text{TiO}_2$  unsintered and sintered targets at 1000 °C. It clearly indicates the transformation of the anatase phase (anatase  $\text{TiO}_2$ , ICSD file no. 01-089-4921) with particle sizes of 47.9 nm dominant in the unsintered target (25 °C) of  $\text{TiO}_2$  to the rutile phase (Rutile  $\text{TiO}_2$ -ICSD file no. 01-087-0710) with particle sizes of 41.7 nm in the 1000 °C sintered target, due to the high sintering temperature, according to the current literature [14,15]. However, in the unsintered target,  $\text{Ti}_3\text{O}_5$  peaks ( $\text{Ti}_3\text{O}_5$ -PDF file no. 96-152-7091) are also observed as secondary phases, which could be converted partially to  $\text{Ti}_6\text{O}$  ( $\text{Ti}_6\text{O}$ -ICSD file no. 01-072-1471) in the target sintered at 1000 °C, due to the oxygen deficiency during the sintering process [20].

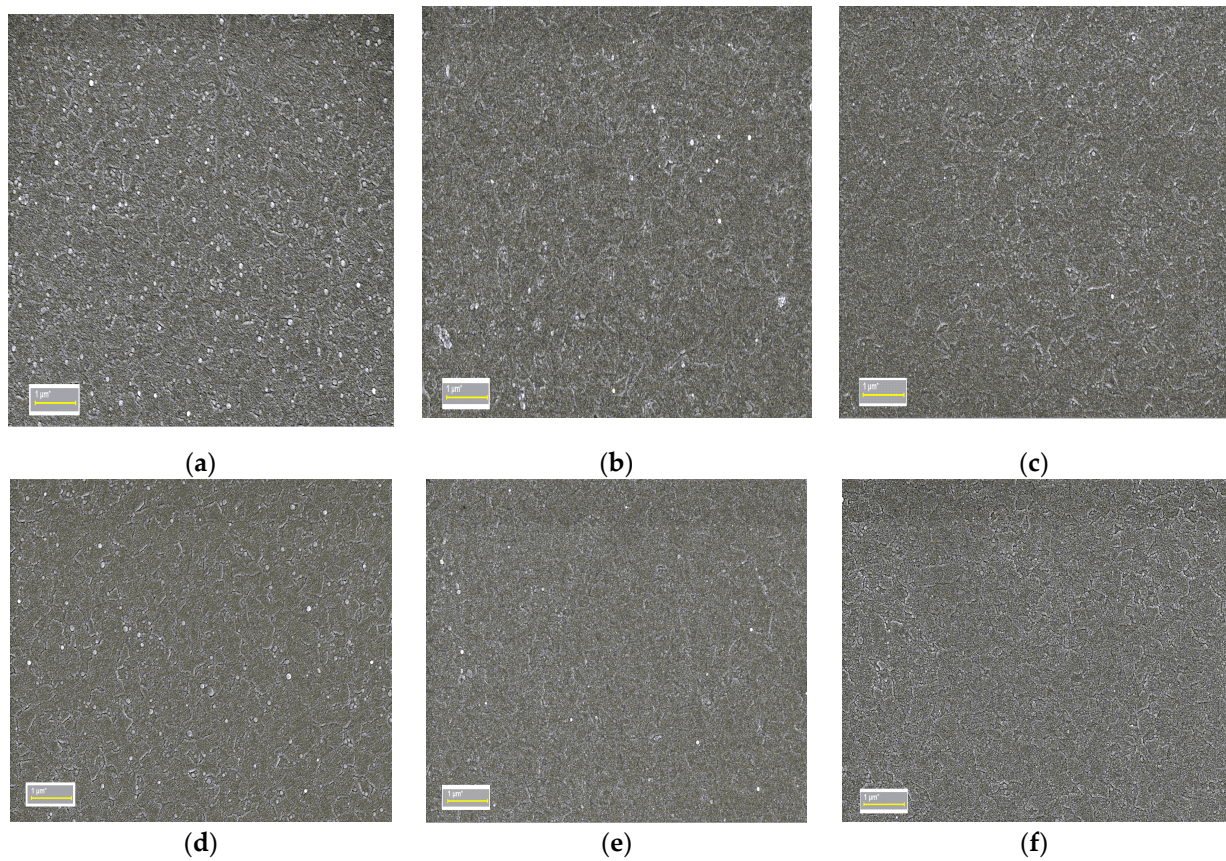


**Figure 2.** SEM images of  $\text{TiO}_2$  thin films grown on ITO glass substrates by PLD, from targets sintered at different temperatures: (a) as 25- $\text{TiO}_2$ , (b) as 500- $\text{TiO}_2$ , (c) as 1000- $\text{TiO}_2$ , (d) ptt 25- $\text{TiO}_2$ , (e) ptt 500- $\text{TiO}_2$  and (f) ptt 1000- $\text{TiO}_2$ .

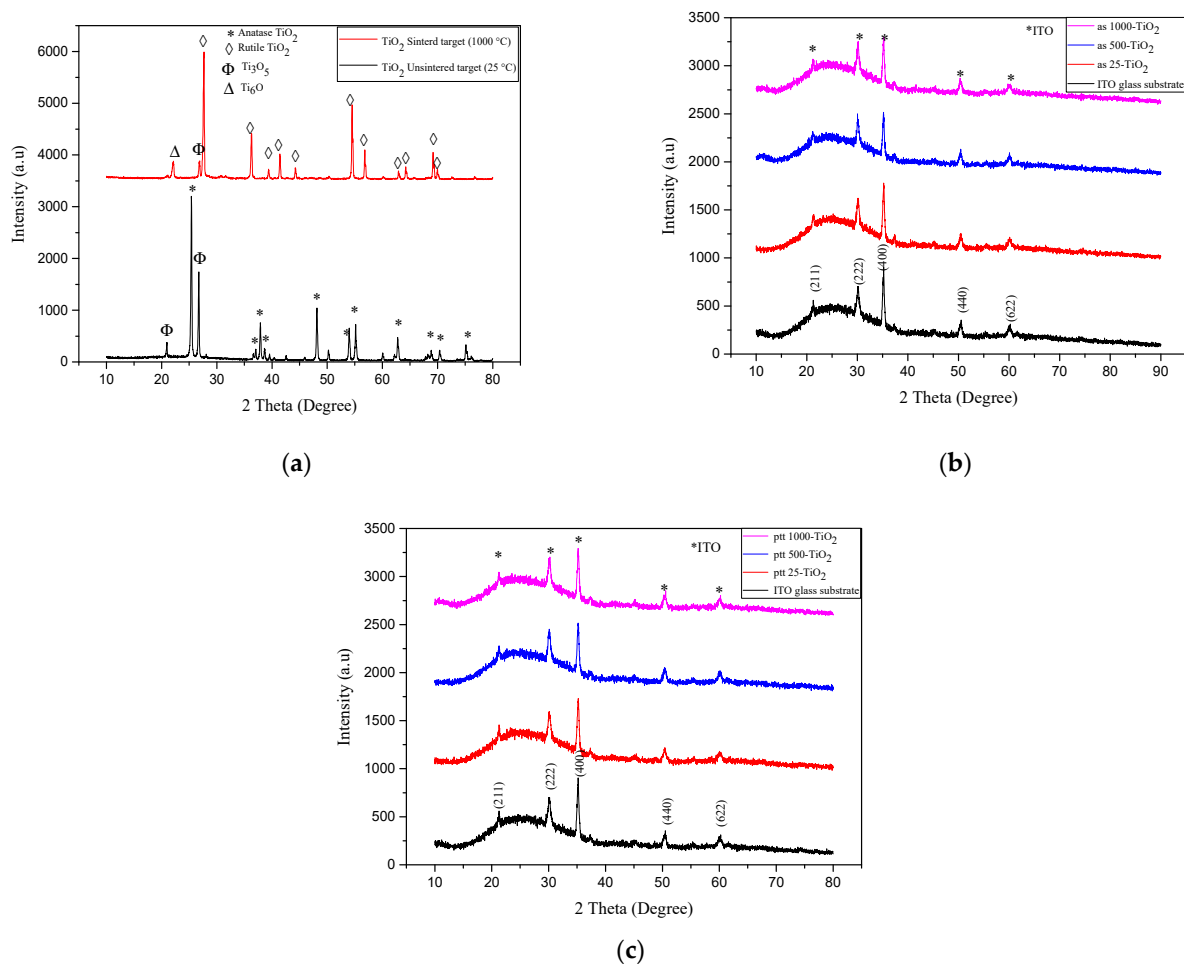
On the other hand, the XRD patterns of the samples and ITO glass substrate before and after heat treatment at 150 °C for 30 min are presented in Figure 3b,c, respectively. It can be clearly noticed that the ITO (ITO-ICSD file no. 01-089-4596) glass substrates exhibit the (400) preferred orientation, and consequently, this plane contains more oxygen vacancies than the (222) one [42]. As can be easily observed, all diffractograms exhibit no obvious diffraction peak except those corresponding to the ITO glass substrate, suggesting that nanosized  $\text{TiO}_2$  films under study, both untreated and heat treated, are amorphous. The broad amorphous halo between 15° and 40° is mainly due to the amorphous glass substrate, as well as to the amorphous  $\text{TiO}_2$  phase. The thermal treatment of titania thin-film samples, conducted at 150 °C for 30 min, is most likely not sufficient to result in a detectable crystallization [1].

### 3.3. Optical Properties

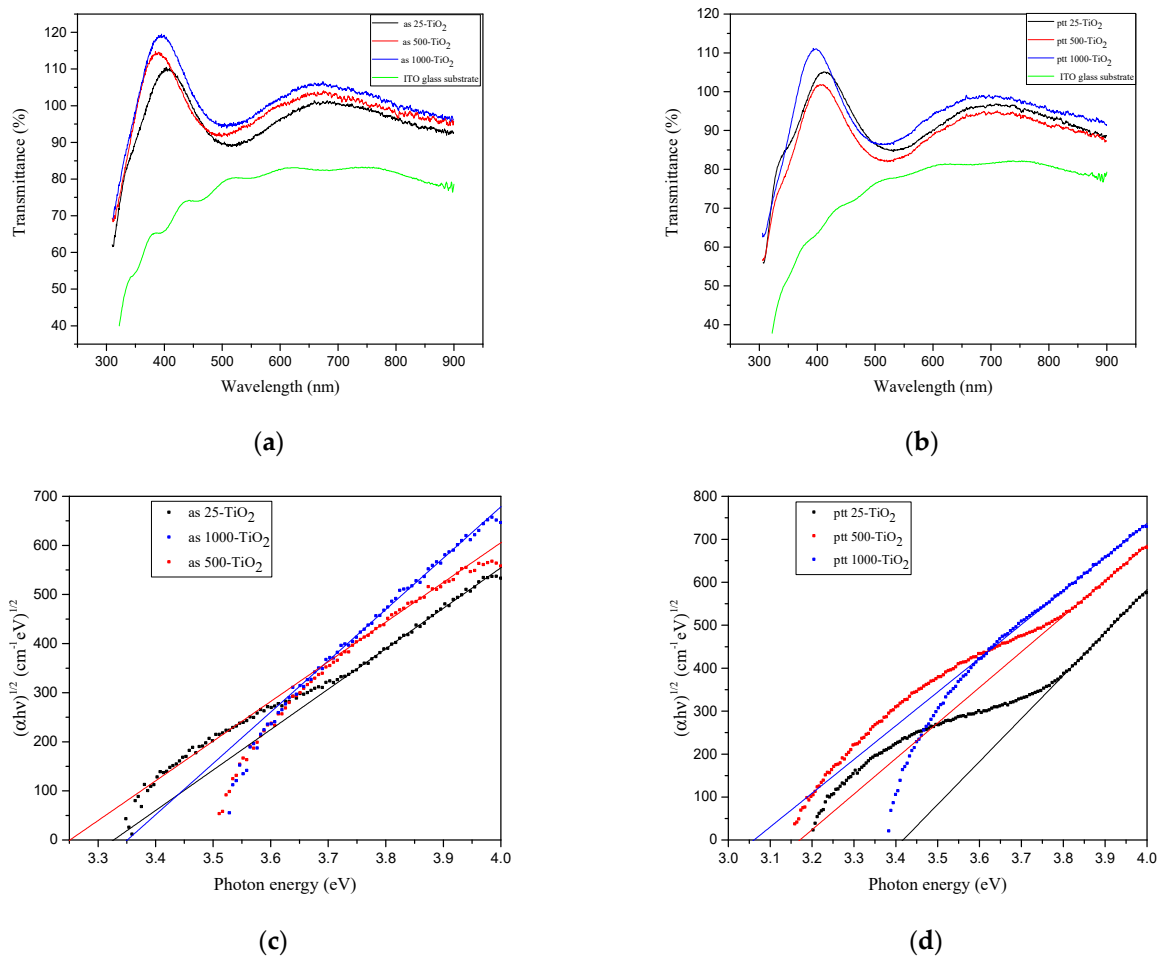
In order to investigate the effect of target sintering temperatures on the optical properties of titanium dioxide thin films, optical transmittance and optical band gap studies were performed in the UV–visible region.

Figure 4 shows the UV–vis transmittance spectra of  $\text{TiO}_2$  thin films and ITO glass substrate reference before (Figure 4a) and after thermal treatment (Figure 4b). In the spectral range from 300 nm to 400 nm, the transmittances increased from 60% to 120% and from 55% to 110% for as deposited and post-thermally treated films, respectively. The transmissions were approximately 100% for as-deposited films and 95% for thermally treated films in the visible range. The transmission of as-deposited films in the visible range can be conditioned by the large band gap of amorphous  $\text{TiO}_2$  [1]. However, the transmission in the UV region and high transmission in the visible range, particularly that which exceeds 100%, remain ambiguous. This can be explained by sample photoluminescence, PL (i.e., when irradiated,  $\text{TiO}_2$  nanostructures exhibit luminescence emission, which may increase

the transmittance intensity), which is strongly related to the presence of surface states and defects [41], whereas amorphous  $\text{TiO}_2$  displays high defect density and disordered arrangement, as mentioned in the introduction. Moreover, amorphous  $\text{TiO}_2$  nanoparticles exhibit a green PL band that is almost always visible, and highlighted the potential for PL-based applications using amorphous  $\text{TiO}_2$  nanoparticles [41]. As a result, and more often, one can observe PL emissions in the UV region of transmittance spectra. Thus,  $\text{TiO}_2$  thin films display originally high transmittance in the visible range, and nanostructured  $\text{TiO}_2$  thin films are able to emit a luminescence spectrum under light excitation, which can result in transmittance intensities higher than 100%. The oscillations present (two main bands with maxima in the visible range) in transmittance spectra of both untreated and thermally treated films are interference-based effects (interference of reflected light from both faces of the film) [43]. The interference fringes suggest that examined films are optically plane, homogeneous and display smooth surfaces [15,43]. In the UV–vis region, the transmittance of  $\text{TiO}_2$  films, thermally treated at  $150^\circ\text{C}$  for 30 min, decreased slightly compared to that of the as-deposited films, and became reasonable in the visible spectrum range, due to scattering enhancement after thermal treatment [44]. Additionally, the transmittance of *ptt500-TiO<sub>2</sub>* film was found to decrease more sharply compared to the others. This decrease might be the result of the increased surface roughness of thinner films, in the presence of mentioned cracks and agglomerations. The films from sintered targets exhibit slightly higher transmittance than those prepared at the room temperature ( $25^\circ\text{C}$ ) pressed target, owing to their lower thickness [45]. Hence, the optical transmittance is proportional to the target sintering temperature.



**Figure 3.** XRD patterns: (a) unsintered and  $1000^\circ\text{C}$  sintered target, and PLD  $\text{TiO}_2$  thin films on ITO glass substrates; (b) before and (c) after thermal treatment at  $150^\circ\text{C}$  for 30 min.



**Figure 4.** (a,b) UV–vis transmittance spectra of TiO<sub>2</sub> thin films and ITO glass substrate, (c,d) band gap energy determination (Tauc plot) of TiO<sub>2</sub> thin films deposited by PLD from targets sintered at different temperatures: (a,c) as-deposited and (b,d) after thermal treatment (150 °C for 30 min).

The optical band gap,  $E_g$ , was calculated using the Tauc equation for indirect transitions [22,46]:

$$(\alpha hv)^{1/2} = k(hv - E_g) \quad (1)$$

where  $\alpha$  denotes the optical absorption coefficient, defined as  $\alpha = \left[ \frac{1}{d} \ln\left(\frac{1}{T}\right) \right]$  (under the assumption of a negligible reflectance,  $R \ll 1$ ),  $d$  is the film thickness,  $T$  is the transmittance,  $hv$  is the photon energy and  $k$  is a constant. The optical band gap was estimated at the absorption edge, by extrapolating the linear part of the  $(\alpha hv)^{1/2} = f(hv)$  plots to zero absorption [43], as shown in Figure 4c,d for as-deposited and thermally treated thin films, respectively. The estimated band gaps ( $E_g$ ) are summarized in Table 2.

As can be inferred from the data listed in Table 2, the  $E_g$  values of the as-deposited amorphous nanosized TiO<sub>2</sub> films ranged between 3.25 eV and 3.35 eV, in good agreement with those reported by Zhang et al. [43] and Addonizio et al. [1] for amorphous TiO<sub>2</sub> films. After thermal treatment, the  $E_g$  value of the compact layers deposited from sintered targets decreased due to the change in the thin-film nanostructure (density) [44]. On the contrary, *pvt* 25-TiO<sub>2</sub> showed a slight increase in  $E_g$  value, which could be caused by an artifact of the nanostructure [15]. As one can observe, the optical band gap of *pvt* 500-TiO<sub>2</sub> film (3.17 eV) is closer to that of anatase TiO<sub>2</sub> {3.20 eV [47]}, confirmed by Sirgh et al. [48] and Sun et al. [24], while the  $E_g$  value of *pvt*1000-TiO<sub>2</sub> (3.06 eV) is much closer to that of rutile TiO<sub>2</sub> {3.02–3.05 eV[47]}. In this way, amorphous TiO<sub>2</sub>-based nanostructures can provide a promising method for overcoming crystalline titania crystalline-related challenges.

**Table 2.** The estimated band gaps ( $E_g$ ) of TiO<sub>2</sub> thin films deposited from unsintered and sintered targets, before and after thermal treatment.

	As-Deposited			Post-Thermal Treatment		
	25	500	1000	25	500	1000
Sintering temperature (°C)	25	500	1000	25	500	1000
Film thickness, $d$ (nm)	67	47	34	67	47	34
Optical band gap, $E_g$ (eV)	3.32	3.25	3.35	3.41	3.17	3.06

#### 4. Conclusions

In this work, the properties of TiO<sub>2</sub> thin films deposited by the PLD technique were examined. The effect of target sintering temperature on the morphological and optical characteristics of titania thin films was investigated in detail. The results showed that amorphous nanosized TiO<sub>2</sub> films from sintered targets can be successfully prepared via PLD with actual deposition parameters. Profilometer measurements demonstrated that TiO<sub>2</sub> thin film thicknesses obtained from sintered targets are more reliable than those obtained from unsintered target. SEM characterization revealed flat and relatively good homogeneity of the nanosized films from sintered targets, and the presence of small cracks and agglomerates in the film from the unsintered target. A correlation between the target sintering temperature and film morphology was observed: thinner films from higher sintering temperature targets (more than 500 °C) can assure good adherence of the titania films; however, sparse targets (below 500 °C) provoke agglomerate formation on the film surfaces. The low temperature thermal treatment (30 min at 150 °C) of the nanosized TiO<sub>2</sub> films led to a reduction in particulates in the film prepared from unsintered target. The TiO<sub>2</sub> thin films exhibited high transparency in the visible range, which corresponded to the large band gap and was proportional to the sintering temperature of target. In addition, the optical transmission was moderate in the visible range, and the optical band gaps of the films prepared from 500 °C and 1000 °C sintered targets were found to be similar to those of anatase and rutile TiO<sub>2</sub> phases, respectively, which offers a promising perspective on the challenges of amorphous TiO<sub>2</sub>-based nanostructures.

**Author Contributions:** Conceptualization, L.K.; Data curation, L.K., G.B., A.C., S.G. (Stoian George) and C.D.; Investigation, L.K., L.L., A.C.; Resources, G.B., A.C., S.G. (Stoian George), S.G. (Silviu Gurlui), L.L. and C.D.; Supervision, S.G. (Stoian George), L.L., C.D. and M.A.; Writing—original draft, L.K.; Writing—review & editing, G.B., A.C., L.L., C.D. and M.A. All authors have read and agreed to the published version of the manuscript.

**Funding:** This research was funded by Ministry of Research, Innovation and Digitization, project FAIR\_09/24.11.2020 and by the Executive Agency for Higher Education, Research, Development, and Innovation, UEFISCDI, ROBIM- project number PN-III-P4-ID-PCE2020-0332.

**Institutional Review Board Statement:** Not applicable.

**Informed Consent Statement:** Not applicable.

**Acknowledgments:** The authors would like to acknowledge all participants from Electron Microscopy and Materials Sciences Laboratory (LMESM) at Oran University of Sciences and Technology -Mohamed Boudiaf (USTO-MB) in Algeria, as well as Atmosphere Optics, Spectroscopy and Lasers Laboratory (LOA-SL) and CERNESIM research center at Alexandru Ioan Cuza University of Iasi in Romania, for their help in the synthesis and characterization of samples, as well as for their insightful discussions. The first author gratefully acknowledges the Faculty of Physics at Alexandru Ioan Cuza University of Iasi in Romania and Faculty of Physics at USTO-MB for the research fellowship offered at the Alexandru Ioan Cuza University of Iasi, Romania.

**Conflicts of Interest:** The authors declare no conflict of interest.

## References

1. Addonizio, M.L.; Aronne, A.; Imparato, C. Amorphous hybrid TiO<sub>2</sub> thin films: The role of organic ligands and UV irradiation. *Appl. Surf. Sci.* **2020**, *502*, 144095. [[CrossRef](#)]
2. Deng, Y.; Ma, Z.; Ren, F.; Wang, G. Improved photoelectric performance of DSSCs based on TiO<sub>2</sub> nanorod array/Ni-doped TiO<sub>2</sub> compact layer composites film. *J. Solid State Electrochem.* **2019**, *23*, 3031–3041. [[CrossRef](#)]
3. Rosales, A.; Esquivel, K. SiO<sub>2</sub>@TiO<sub>2</sub> composite synthesis and its hydrophobic applications: A review. *Catalysts* **2020**, *10*, 171. [[CrossRef](#)]
4. Cheng, X.; Shang, Y.; Cui, Y.; Shi, R.; Zhu, Y.; Yang, P. Enhanced photoelectrochemical and photocatalytic properties of anatase-TiO<sub>2</sub>(B) nanobelts decorated with CdS nanoparticles. *Solid State Sci.* **2020**, *99*. [[CrossRef](#)]
5. Wang, K.; Janczarek, M.; Wei, Z.; Raja-Mogan, T.; Endo-Kimura, M.; Khedr, T.M.; Ohtani, B.; Kowalska, E. Morphology- and crystalline composition-governed activity of titania-based photocatalysts: Overview and perspective. *Catalysts* **2019**, *9*, 1054. [[CrossRef](#)]
6. Tobaldi, D.M.; Lajaunie, L.; Rozman, N.; Caetano, A.P.F.; Seabra, M.P.; Sever Škapin, A.; Arenal, R.; Labrincha, J.A. Impact of the absolute rutile fraction on TiO<sub>2</sub> visible-light absorption and visible-light-promoted photocatalytic activity. *J. Photochem. Photobiol. A Chem.* **2019**, *382*, 111940. [[CrossRef](#)]
7. Zarhri, Z.; Avilés Cardos, M.Á.; Ziat, Y.; Hammi, M.; El Rhazouani, O.; Cruz Argüello, J.C.; Avellaneda Avellaneda, D. Synthesis, structural and crystal size effect on the optical properties of sprayed TiO<sub>2</sub> thin films: Experiment and DFT TB-mbj. *J. Alloys Compd.* **2020**, *819*, 153010. [[CrossRef](#)]
8. Murugesan, S.; Kuppasami, P.; Parvathavarthini, N.; Mohandas, E. Pulsed laser deposition of anatase and rutile TiO<sub>2</sub> thin films. *Surf. Coat. Technol.* **2007**, *201*, 7713–7719. [[CrossRef](#)]
9. Wang, B.; Yang, J.; Lu, L.; Xiao, W.; Wu, H.; Xiong, S.; Tang, J.; Duan, C.; Bao, Q. Interface Engineering of Air-Stable n-Doping Fullerene-Modified TiO<sub>2</sub> Electron Transport Layer for Highly Efficient and Stable Perovskite Solar Cells. *Adv. Mater. Interfaces* **2020**, *7*, 1901964. [[CrossRef](#)]
10. Liu, Y.; Xu, C.; Xie, Y.; Yang, L.; Ling, Y.; Chen, L. Au–Cu nanoalloy/TiO<sub>2</sub>/MoS<sub>2</sub> ternary hybrid with enhanced photocatalytic hydrogen production. *J. Alloys Compd.* **2020**, *820*, 153440. [[CrossRef](#)]
11. Hajjaji, A.; Jemai, S.; Trabelsi, K.; Kouki, A.; Ben Assaker, I.; Ka, I.; Gaidi, M.; Bessais, B.; El Khakani, M.A. Study of TiO<sub>2</sub> nanotubes decorated with PbS nanoparticles elaborated by pulsed laser deposition: Microstructural, optoelectronic and photoelectrochemical properties. *J. Mater. Sci. Mater. Electron.* **2019**, *30*, 20935–20946. [[CrossRef](#)]
12. Li, M.Y.; Yu, M.; Su, D.; Zhang, J.; Jiang, S.; Wu, J.; Wang, Q.; Liu, S. Ultrahigh Responsivity UV Photodetector Based on Cu Nanostructure/ZnO QD Hybrid Architectures. *Small* **2019**, *15*, 1901606. [[CrossRef](#)] [[PubMed](#)]
13. Liu, S.; Li, M.Y.; Zhang, J.; Su, D.; Huang, Z.; Kunwar, S.; Lee, J. Self-Assembled Al Nanostructure/ZnO Quantum Dot Heterostructures for High Responsivity and Fast UV Photodetector. *Nano-Micro Lett.* **2020**, *12*. [[CrossRef](#)]
14. Timoumi, A.; Albetran, H.M.; Alamri, H.R.; Alamri, S.N.; Low, I.M. Impact of annealing temperature on structural, morphological and optical properties of GO-TiO<sub>2</sub> thin films prepared by spin coating technique. *Superlattices Microstruct.* **2020**, *139*, 106423. [[CrossRef](#)]
15. Kabir, I.I.; Sheppard, L.R.; Shamiri, R.; Koshy, P.; Liu, R.; Joe, W.; Le, A.; Lu, X.; Chen, W.F.; Sorrell, C.C. Contamination of TiO<sub>2</sub> thin films spin coated on borosilicate and rutile substrates. *J. Mater. Sci.* **2020**, *55*, 3774–3794. [[CrossRef](#)]
16. Wang, S.J.; Chang, W.-T.; Ciou, J.-Y.; Wei, M.-K.; Wong, M.S. Preparation of TiO<sub>2</sub> thin films by laser ablation for photocatalytic applications. *J. Vac. Sci. Technol. A Vac. Surfaces Film* **2008**, *26*, 898–902. [[CrossRef](#)]
17. Kim, I.S.; Haasch, R.T.; Cao, D.H.; Farha, O.K.; Hupp, J.T.; Kanatzidis, M.G.; Martinson, A.B.F. Amorphous TiO<sub>2</sub> Compact Layers via ALD for Planar Halide Perovskite Photovoltaics. *ACS Appl. Mater. Interfaces* **2016**, *8*, 24310–24314. [[CrossRef](#)]
18. Murugesan, S.; Padhy, N.; Kuppasami, P.; Mudali, U.K.; Mohandas, E. A study of structural transition in nanocrystalline titania thin films by X-ray diffraction Rietveld method. *Mater. Res. Bull.* **2010**, *45*, 1973–1977. [[CrossRef](#)]
19. Zhang, H.; Wang, H.; Ma, M.; Wu, Y.; Dong, S.; Xu, Q. Application of Compact TiO<sub>2</sub> Layer Fabricated by Pulsed Laser Deposition in Organometal Trihalide Perovskite Solar Cells. *Sol. RRL* **2018**, *2*, 1800097. [[CrossRef](#)]
20. Nakamura, T.; Ichitubo, T.; Matsubara, E.; Muramatsu, A.; Sato, N.; Takahashi, H. Preferential formation of anatase in laser-ablated titanium dioxide films. *Acta Mater.* **2005**, *53*, 323–329. [[CrossRef](#)]
21. Shriwastava, S.K.; Singh, S. Effect & Growth of TiO<sub>2</sub> Thin Films for Solar Cell Applications. *Int. J. Hybrid. Inf. Technol.* **2016**, *9*, 267–274. [[CrossRef](#)]
22. Jia, T.; Zhang, J.; Wu, J.; Wang, D.; Liu, Q.; Qi, Y.; Hu, B.; He, P.; Pan, W.; Qi, X. Synthesis amorphous TiO<sub>2</sub> with oxygen vacancy as carriers transport channels for enhancing photocatalytic activity. *Mater. Lett.* **2020**, *265*. [[CrossRef](#)]
23. Liu, Z.S.; Xu, J.W. Fabrication of BiO<sub>2</sub>-x@TiO<sub>2</sub> heterostructures with enhanced photocatalytic activity and stability. *Appl. Surf. Sci.* **2020**, *511*. [[CrossRef](#)]
24. Sun, S.; Song, P.; Cui, J.; Liang, S. Amorphous TiO<sub>2</sub> nanostructures: Synthesis, fundamental properties and photocatalytic applications. *Catal. Sci. Technol.* **2019**, *9*, 4198–4215. [[CrossRef](#)]
25. Pulker, H.K.; Paesold, G.; Ritter, E. Refractive indices of TiO<sub>2</sub> films produced by reactive evaporation of various titanium–oxygen phases. *Appl. Opt.* **1976**, *15*, 2986. [[CrossRef](#)] [[PubMed](#)]
26. Wang, S.F.; Hsu, Y.F.; Lee, Y.S. Microstructural evolution and optical properties of doped TiO<sub>2</sub> films prepared by RF magnetron sputtering. *Ceram. Int.* **2006**, *32*, 121–125. [[CrossRef](#)]

27. Sun, H.; Wang, C.; Pang, S.; Li, X.; Tao, Y.; Tang, H.; Liu, M. Photocatalytic TiO<sub>2</sub> films prepared by chemical vapor deposition at atmosphere pressure. *J. Non. Cryst. Solids* **2008**, *354*, 1440–1443. [[CrossRef](#)]
28. Vorotilov, K.A.; Orlova, E.V.; Petrovsky, V.I. Sol.-gel TiO<sub>2</sub> Films on Silicon Substrates. *Thin Solid Films* **1992**, *207*, 180–184. [[CrossRef](#)]
29. György, E.; Socol, G.; Axente, E.; Mihailescu, I.N.; Ducu, C.; Ciuca, S. Anatase phase TiO<sub>2</sub> thin films obtained by pulsed laser deposition for gas sensing applications. *Appl. Surf. Sci.* **2005**, *247*, 429–433. [[CrossRef](#)]
30. Shimizu, R.; Sugiyama, I.; Nakamura, N.; Kobayashi, S.; Hitosugi, T. Pulsed laser deposition of oxide thin films by the fifth harmonic of a Nd:Y3Al5O12 (Nd:YAG) laser. *AIP Adv.* **2018**, *8*, 095101. [[CrossRef](#)]
31. Abdulraheem, Y.M.; Ghorraishi, S.; Arockia-Thai, L.; Zachariah, S.K.; Ghannam, M. The effect of annealing on the structural and optical properties of titanium dioxide films deposited by electron beam assisted PVD. *Adv. Mater. Sci. Eng.* **2013**, *2013*, 574738. [[CrossRef](#)]
32. Meng, L.; Wang, Z.; Yang, L.; Ren, W.; Liu, W.; Zhang, Z.; Yang, T.; dos Santos, M.P. A detailed study on the Fe-doped TiO<sub>2</sub> thin films induced by pulsed laser deposition route. *Appl. Surf. Sci.* **2019**, *474*, 211–217. [[CrossRef](#)]
33. Irimiciuc, S.A.; Hodoroaba, B.C.; Bulai, G.; Gurlui, S.; Craciun, V. Multiple structure formation and molecule dynamics in transient plasmas generated by laser ablation of graphite. *Spectrochim. Acta Part B At. Spectrosc.* **2020**, *165*. [[CrossRef](#)]
34. Agop, M.; Cimpoesu, N.; Gurlui, S.; Irimiciuc, S.A. Investigations of transient plasma generated by laser ablation of hydroxyapatite during the pulsed laser deposition process. *Symmetry* **2020**, *12*, 132. [[CrossRef](#)]
35. Mascaretti, L.; Matarrese, R.; Ravanelli, A.; Isacchi, M.; Mazzolini, P.; Casari, C.S.; Russo, V.; Nova, I.; Terraneo, G.; Ducati, C.; et al. Tuning the photoelectrochemical properties of hierarchical TiO<sub>2</sub> nanostructures by control of pulsed laser deposition and annealing in reducing conditions. *Int. J. Hydrog. Energy* **2017**, *42*, 26639–26651. [[CrossRef](#)]
36. Kim, J.H.; Lee, S.; Im, H.S. Effect of Target Density and Its Morphology on TiO<sub>2</sub> Thin Films Grown on Si(100) By PLD. *Appl. Surf. Sci.* **1999**, *151*, 6–16. [[CrossRef](#)]
37. Yang, B.; Mahjouri-Samani, M.; Rouleau, C.M.; Geohegan, D.B.; Xiao, K. Low temperature synthesis of hierarchical TiO<sub>2</sub> nanostructures for high performance perovskite solar cells by pulsed laser deposition. *Phys. Chem. Chem. Phys.* **2016**, *18*, 27067–27072. [[CrossRef](#)]
38. Huo, X.; Jiang, S.; Liu, P.; Shen, M.; Qiu, S.; Li, M.Y. Molybdenum and tungsten doped SnO<sub>2</sub> transparent conductive thin films with broadband high transmittance between the visible and near-infrared regions. *CrystEngComm* **2017**, *19*, 4413–4423. [[CrossRef](#)]
39. Bulai, G.; Trandafir, V.; Irimiciuc, S.A.; Ursu, L.; Focsa, C.; Gurlui, S. Influence of rare earth addition in cobalt ferrite thin films obtained by pulsed laser deposition. *Ceram. Int.* **2019**, *45*, 20165–20171. [[CrossRef](#)]
40. Ogugua, S.N.; Ntwaeaborwa, O.M.; Swart, H.C. Latest development on pulsed laser deposited thin films for advanced luminescence applications. *Coatings* **2020**, *10*, 1078. [[CrossRef](#)]
41. Pallotti, D.K.; Orabona, E.; Amoroso, S.; Aruta, C.; Bruzzese, R.; Chiarella, F.; Tuzi, S.; Maddalena, P.; Lettieri, S. Multi-band photoluminescence in TiO<sub>2</sub> nanoparticles-assembled films produced by femtosecond pulsed laser deposition. *J. Appl. Phys.* **2013**, *114*, 043503. [[CrossRef](#)]
42. Kosarian, A.; Shakiba, M.; Farshidi, E. Role of sputtering power on the microstructural and electro-optical properties of ITO thin films deposited using DC sputtering technique. *IEEE Trans. Electr. Electron. Eng.* **2018**, *13*, 27–31. [[CrossRef](#)]
43. Zhang, M.; Lin, G.; Dong, C.; Wen, L. Amorphous TiO<sub>2</sub> films with high refractive index deposited by pulsed bias arc ion plating. *Surf. Coat. Technol.* **2007**, *201*, 7252–7258. [[CrossRef](#)]
44. Ben Naceur, J.; Gaidi, M.; Bousbih, F.; Mechiakh, R.; Chtourou, R. Annealing effects on microstructural and optical properties of Nanostructured-TiO<sub>2</sub> thin films prepared by sol-gel technique. *Curr. Appl. Phys.* **2012**, *12*, 422–428. [[CrossRef](#)]
45. Anitha, V.C.; Banerjee, A.N.; Joo, S.W. Recent developments in TiO<sub>2</sub> as n- and p-type transparent semiconductors: Synthesis, modification, properties, and energy-related applications. *J. Mater. Sci.* **2015**, *50*, 7495–7536. [[CrossRef](#)]
46. Sreemany, M.; Sen, S. A simple spectrophotometric method for determination of the optical constants and band gap energy of multiple layer TiO<sub>2</sub> thin films. *Mater. Chem. Phys.* **2004**, *83*, 169–177. [[CrossRef](#)]
47. Möls, K.; Aarik, L.; Mändar, H.; Kasikov, A.; Niilisk, A.; Rammula, R.; Aarik, J. Influence of phase composition on optical properties of TiO<sub>2</sub>: Dependence of refractive index and band gap on formation of TiO<sub>2</sub>-II phase in thin films. *Opt. Mater. (Amst.)* **2019**, *96*, 109335. [[CrossRef](#)]
48. Sirghi, L.; Hatanaka, Y. Hydrophilicity of amorphous TiO<sub>2</sub> ultra-thin films. *Surf. Sci.* **2003**, *530*, L323–L327. [[CrossRef](#)]